minerals

MDPI

Article

Structural and Chemical Diversity and Complexity of Sulfur Minerals

Vladimir G. Krivovichev [1], Sergey V. Krivovichev [2,3,*] and Galina L. Starova [3]

[1] Department of Mineralogy, Institute of Earth Sciences, St. Petersburg State University, University Emb. 7/9, 199034 St. Petersburg, Russia; v.krivovichev@spbu.ru
[2] Nanomaterials Research Centre, Kola Science Centre, Russian Academy of Sciences, Fersmana 14, 184209 Apatity, Russia
[3] Department of Crystallography, Institute of Earth Sciences, St. Petersburg State University, University Emb. 7/9, 199034 St. Petersburg, Russia; glstarova@yandex.ru
* Correspondence: s.krivovichev@ksc.ru

Abstract: The chemical and structural diversity of minerals containing sulfur as an essential mineral-forming element has been analyzed in terms of the concept of mineral systems and the information-based structural and chemical complexity parameters. The study employs data for 1118 sulfur mineral species approved by the International Mineralogical Association. All known sulfur minerals belong to nine mineral systems, with the number of essential components ranging from one to nine. The chemical and structural complexity of S minerals correlate with each other; that is, on average, chemical complexification results in structural complexification. The minerals with S–O bonds (sulfates and sulfites) are more complex than those without S–O bonds (sulfides and sulfosalts). However, the most complex sulfur mineral known so far is incomsartorite, $Tl_6Pb_{144}As_{246}S_{516}$, a sulfosalt. The complexity-generating mechanism in sulfides and sulfosalts is the complex combination of different modules excised from parent PbS or SnS archetypes with the subsequent formation of superstructures. The drivers for structural complexity in sulfates are more diverse and, in addition to modular construction and superstructures, also include a high hydration state, the presence of polyatomic clusters, and framework complexity. The most complex Martian minerals are most probably halotrichite-group minerals. The chemical and structural complexity increases with the passage of geological time with the formation of the most complex sulfosalts at Lengenbach (Swiss Alps) triggered by life (activity of sulfur-reducing bacteria).

Keywords: sulfur; sulfides; sulfosalts; sulfates; structural complexity; chemical complexity; information measures

check for updates

Citation: Krivovichev, V.G.; Krivovichev, S.V.; Starova, G.L. Structural and Chemical Diversity and Complexity of Sulfur Minerals. *Minerals* **2023**, *13*, 1069. https://doi.org/10.3390/min13081069

Academic Editor: Jiří Sejkora

Received: 16 July 2023
Revised: 9 August 2023
Accepted: 10 August 2023
Published: 12 August 2023

Copyright: © 2023 by the authors. Licensee MDPI, Basel, Switzerland. This article is an open access article distributed under the terms and conditions of the Creative Commons Attribution (CC BY) license (https://creativecommons.org/licenses/by/4.0/).

1. Introduction

Sulfur is the tenth most abundant element in the Solar system [1] and the thirteenth in the Earth's continental crust [2]. The global sulfur cycle is of primary biogeochemical importance due to the biological role of S as a component of proteins. Sulfur is a highly reactive element that may form ions with different oxidation states: S^{2-} in sulfides, S^0 in elementary sulfur, S^{4+} in sulfites, and S^{6+} in sulfates. Metal sulfides are essential raw materials for modern industry and have long been considered important ore minerals [3]. The oxidation of sulfides under environmental conditions results in the formation of sulfates, which are important components of acid mine drainage solutions. On the other hand, the reduction of sulfates (e.g., in marine sediments) by microorganisms results in the formation of sulfides, with pyrite being the most important species. The renewed interest in sulfates and sulfur minerals, in general, is due to the remote sensing discovery of sulfates on Mars [4–6] that resulted in a large number of studies on their composition, structure, stability, and abundance under different thermodynamic conditions [7–20], etc. Synthetic analogues of sulfide minerals are known as important high-tech materials (for instance,

kesterite-type compounds are used in solar cell technologies [21,22], etc.). Sulfur mineralogy is a mature field of science, with two voluminous review collections being published by the Mineralogical Society of America [23,24]. The crystal chemistry of sulfides and sulfates has been reviewed by Makovicky [25] and Hawthorne et al. [26], respectively.

Sulfur minerals constitute 20.5% of the total number of mineral species. In general, mineral abundances in the Earth's crust are proportional to atomic ones. At the same time, for a number of elements, there is a sharp discrepancy between mineral and atomic abundances in the Earth's crust. Such elements include sulfur, the atomic abundance in the Earth's crust of which differs sharply from ones of aluminum (227 and 63,400 ppm, respectively), whereas the mineral abundances of these elements are approximately equal (20.50 and 19.39%, respectively). There are many reasons for such inconsistencies, and apparently, with the generally positive trend of increasing the number of mineral species of an element with an increase in its atomic abundance, there are a number of factors complicating this dependence for a number of elements [27].

There are 1118 sulfur-containing mineral species presently approved by the International Mineralogical Association (IMA) [28]. About half of known S minerals (529) are sulfides and sulfosalts. In most of the oxygen-bearing species, S occurs as S^{4+} and/or S^{6+} cations. Natural sulfites are unstable under oxidizing conditions and transform into sulfates, which explains the rarity of sulfites in nature. In nature, the vast majority of sulfur oxysalts are sulfates, whereas sulfites are very rare (around seven mineral species only). The reverse pattern is observed for Se oxysalts, for which 5 selenates, 1 selenite–selenate, and 40 selenite minerals have been found in nature. The observed difference can be explained by the fact that the reduced forms of Se acids are more stable at higher Eh values than the corresponding forms of S acids [29,30].

The recent developments in evolutionary mineralogy [31–39] led to a refreshing view of the behavior of minerals and mineral-forming environments in the history of the Universe and the Earth in particular. The special part of this endeavor is the study of mineral ecology as a science of mineral diversity and distribution. One of the interesting aspects of this direction of mineralogy is the investigation of the chemical and structural complexity of minerals and their evolution in the course of geological time. Within this approach, minerals are considered 'ideal' crystals with idealized chemical compositions established by the International Mineralogical Association [28]. The application of information-theoretic measures [40–44] allows us to assign to each mineral some unique complexity characteristics (in binary units) that can be further exploited in mineral informatics research using modern digital technologies [45–47]. The information-based complexity characteristics have been applied to the investigations of boron [48,49], selenium [50], and tellurium [51] minerals. The aim of the current study is to provide an overview of the chemical and structural complexities of sulfur minerals in general and to perform a comparative analysis of the complexity of sulfides and sulfates (including sulfites) as mineral species containing sulfur in reduced and oxidized forms, respectively.

2. Materials and Methods

2.1. Mineral Systems

In accordance with the previous studies [52,53], any mineral species can be assigned to a mineral system according to the number of species-defining elements in its chemical formula approved by the IMA in agreement with the current rules for the definition of a new mineral species [54–60]. The chemical formulae of S minerals used to compose mineral systems are taken from V. Krivovichev [61] and the list of IMA-approved mineral species [28]. We identified the mineral system for each sulfur mineral according to its species-defining elements; e.g., for lorándite, $TlAsS_2$, the system is the three-component SAsTl one. Only species-defining elements are taken into account, whereas other isomorphous components are ignored, even geochemically important ones [52,53]. A chemical system is identified in accordance with the thermochemical sequence of chemical elements [52,61,62]. For example, tatarinovite $Ca_3Al(SO_4)[B(OH)_4](OH)_6 \cdot 12H_2O$, belongs

to the system OHBSAlCa, while selenopolybasite $CuAg_6Ag_9Sb_2S_9Se_2$, belongs to the system SSeSbCuAg.

2.2. Chemical and Structural Complexities

To quantify the chemical and structural complexities of sulfur minerals, 1118 pieces of chemical composition data and 941 data sets on crystal structure were reviewed. The level of structural complexity per atom ($^{str}I_G$) and per unit cell ($^{str}I_{G,total}$) [40–44] were calculated using the following equations:

$$^{str}I_G = -\sum_{i=1}^{k} p_i \log_2 p_i (\text{bit/atom}), \quad (1)$$

$$^{str}I_{G,total} = -v\sum_{i=1}^{k} p_i \log_2 p_i (\text{bit/cell}), \quad (2)$$

where k is the number of different crystallographic orbits (Wyckoff sites) in the structure and p_i is the random choice probability for an atom from the ith crystallographic orbit, that is:

$$p_i = m_i/v, \quad (3)$$

where m_i is a multiplicity of a crystallographic orbit (i.e., the number of atoms of a specific Wyckoff site in the reduced unit cell) and v is the total number of atoms in the reduced unit cell.

For several hydrated sulfur minerals, the H sites have not been determined experimentally, and the H-correction procedure has been applied [63]. The structure complexity calculations have been performed using the TOPOS program package [64].

The chemical complexities of sulfur minerals have been evaluated by calculating the amount of chemical information per atom ($^{chem}I_G$) and per formula unit, f.u. ($^{chem}I_{G,total}$). The chemical information was calculated as follows [65]:

$$^{chem}I_G = -\sum_{i=1}^{k} p_i \log_2 p_i (\text{bit/atom}) \quad (4)$$

$$^{chem}I_{G,total} = -e\sum_{i=1}^{k} p_i \log_2 p_i (\text{bit/cell}) \quad (5)$$

where k is the number of species-defining chemical elements, and p_i is the random choice probability for an atom of the ith element, that is:

$$p_i = c_i/e \quad (6)$$

where e is the total number of species-defining elements in the chemical formula:

$$e = \sum_{i=1}^{k} c_i \quad (7)$$

For the calculations of chemical complexities, the ideal chemical formulas of minerals were used.

3. Results and Discussion

3.1. Distribution of S Minerals in Accordance with the Number of Species-Defining Elements

Similarly to the selenium and tellurium minerals [50,51], we divided sulfur minerals into two groups based on their crystal–chemical features: without S–O bonds (sulfides and sulfosalts) and those containing S–O bonds (sulfites and sulfates). The notion about the presence or absence of the S–O bonds is essential since there are several sulfosalts (or oxysulfosalts) such as chovanite, $Pb_{15-2x}Sb_{14+2x}S_{36}O_x$ (x ~0.2), and meerschautite, $Ag_{12}Pb_{84}Sb_{90}S_{224}O$, that contain O^{2-} anions not bonded to S.

The distribution of all sulfur minerals versus the number of species-defining elements, N, is close to normal (Table 1; Figure 1a). The value of N in all sulfur minerals varies from one to nine. All sulfur minerals containing seven or more species-defining

elements were found to be O-bearing. The largest number of minerals was found to consist of four and five species-defining elements (337 and 303 minerals, respectively). The distributions of sulfur minerals within the reduced and oxidized groups depending on the number of species-defining elements, N, are also normal (Table 1; Figure 1b). The arithmetic mean of species-defining elements in reduced S minerals is significantly lower ($\overline{X} = 3.43$; $\sigma_{\overline{X}} = 0.041$) than in oxidized minerals ($\overline{X} = 5.07$; $\sigma_{\overline{X}} = 0.045$). According to the Student's test, the differences in the number of species-forming elements for both groups of S minerals are statistically significant (the confidence level is more than 99.99%).

Table 1. The mineral systems of sulfur minerals.

N	Minerals without S–O Bonds (S^{2-}, S^0)		Minerals with S–O Bonds (S^{4+}, S^{6+})		All S Minerals	
	m_i	p_i	m_i	p_i	m_i	p_i
1	2	0.38	-	-	2	0.18
2	84	15.88	-	-	84	7.51
3	199	37.62	22	4.14	221	19.77
4	177	33.46	160	29.38	337	30.14
5	61	11.53	242	42.94	303	27.10
6	6	1.13	103	17.14	109	9.75
7	-	-	46	5.08	46	4.11
8	-	-	13	1.13	13	1.17
9	-	-	3	0.19	3	0.27
Total	529	100.0	589	100.00	1118	100.0

Note: N—the number of the species-defining elements; m_i—the number of mineral species; $p_i = \left(m_i / \sum_{i=1}^{6} m_i\right) \cdot 100$ —probability, %.

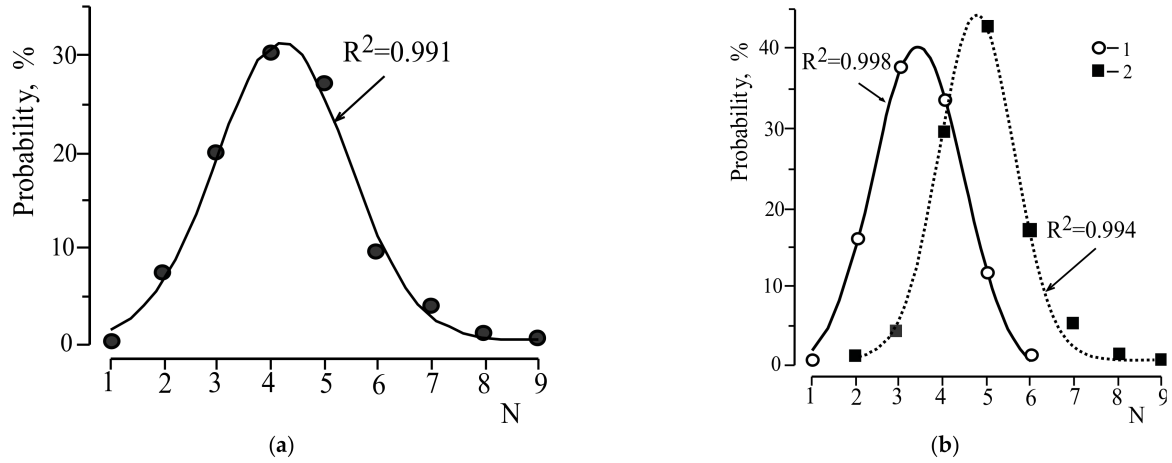


Figure 1. Distribution of sulfur minerals among mineral systems based on the number of the species-defining elements (N): (**a**) all S minerals, (**b**) S minerals without S–O bonds (1, solid line), and S minerals with S–O bonds (2, dashed line).

3.2. Chemical and Structural Complexities of Sulfur Minerals

The information-based complexity parameters of sulfur minerals belonging to different mineral systems (or corresponding to the number N of species-defining chemical elements) were calculated according to Equations (1)–(7). The average chemical and structural complexities of minerals and associated statistical parameters are given in Table 2. The dependencies of different complexities from the value of N were approximated by the following linear functions (Figure 2):

$$^{chem}I_G = 0.436 + 0.217\ N\ (R = 0.881;\ p = 0.002) \quad (8)$$

$$^{str}I_G = 1.736 + 0.374\ N\ (R = 0.877;\ p = 0.002) \quad (9)$$

$$^{chem}I_{G,total} = -59.837 + 28.579\ N\ (R = 0.973;\ p = 4 \times 10^{-5}) \quad (10)$$

$$^{str}I_{G,total} = -96.383 + 107.87\ N\ (R = 0.897;\ p = 0.001) \quad (11)$$

Table 2. Chemical and structural complexities of sulfur minerals according to the number of species-defining chemical elements (N).

N	m_i	$^{chem}I_G$				m_i	$^{str}I_G$			
		[bit/atom]		[bit/f.u.]			[bit/atom]		[bit/cell]	
		$\overline{X}$	$\sigma_{\overline{X}}$	$\overline{X}$	$\sigma_{\overline{X}}$		$\overline{X}$	$\sigma_{\overline{X}}$	$\overline{X}$	$\sigma_{\overline{X}}$
1	3	0	0				2.195	1.35	94.69	66.59
2	87	0.968	0.005	7.33	1.05	78	1.811	0.13	79.52	34.84
3	220	1.420	0.008	17.89	1.36	189	2.549	0.09	107.85	13.94
4	324	1.591	0.008	52.02	3.26	250	3.816	0.08	310.74	21.83
5	293	1.752	0.010	79.87	4.07	229	4.233	0.07	480.35	34.57
6	88	1.780	0.020	107.64	7.84	70	4.298	0.12	527.07	71.81
7	29	1.981	0.034	162.96	18.65	25	3.833	0.16	959.55	209.20
8	5	2.170	0.150	138.35	18.11	4	5.34	0.17	537.67	116.37
9	1	2.026		212.72		1	4.402		889.17	

m_i = number of minerals taken into account; $\overline{X}$ = arithmetic mean; $\sigma_{\overline{X}}$ = standard error of arithmetic mean.

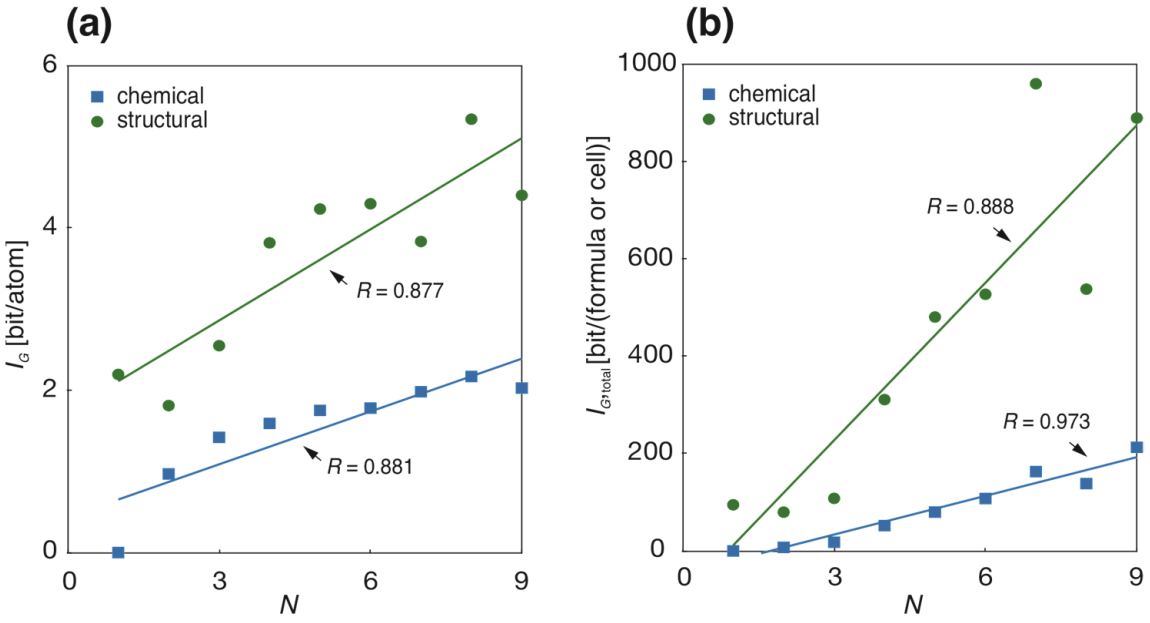


Figure 2. Dependencies of chemical and structural complexities of sulfur minerals on the number of species-defining chemical elements (N): the complexity per atom (**a**) and per unit cell or formula unit (**b**).

The data indicate the existence of statistically significant (a confidence level of more than 99%) and positive relationships (R) between the chemical and structural complexities of S minerals and the number of species-defining chemical elements in their mineral formula, which was also observed for all mineral species in general [65].

The minerals containing no S–O bonds usually form under reducing conditions in endogenous geological formations, whereas sulfites and sulfates based upon SO_n groups

(n = 3, 4) crystallize in oxidizing near-surface environments, both on Earth and Mars. The comparative study of complexity parameters for these two groups of minerals (Table 3) shows that the average arithmetic values of structural and chemical complexities for minerals with reduced forms of sulfur (S^0, S^{2-}) are significantly lower than for those containing S^{4+} and S^{6+} cations. The Student's test [66] shows that the differences are statistically significant.

Table 3. Average structural and chemical complexities of two groups of sulfur minerals.

Complexity Parameters	Without S–O Bonds			With S–O Bonds			Student's *t*-Test	
	m_i	$\overline{X}$	$\sigma_{\overline{X}}$	m_i	$\overline{X}$	$\sigma_{\overline{X}}$	t	p
${}^{chem}I_G$ [bit/atom]	529	1.48	0.01	589	1.67	0.01	13.43	<0.0001
${}^{str}I_G$ [bit/atom]	419	2.88	0.07	522	4.12	0.05	14.42	<0.0001
${}^{chem}I_{G,total}$ [bit/f.u.]	529	39.98	2.63	589	75.24	3.03	8.79	<0.0001
${}^{str}I_{G,total}$ [bit/cell]	419	197.64	15.6	522	460.99	25.46	8.82	<0.0001

m_i = number of minerals taken into account; $\overline{X}$ = arithmetic mean; $\sigma_{\overline{X}}$ = standard error of the arithmetic mean; *p*—probability value or *p*-value.

3.3. Structural Complexity of Sulfur Minerals: Statistics and Mechanisms

The crystal–chemical features and building principles of sulfur minerals strongly depend upon the oxidation state of S, which prompts us to consider the two groups of minerals (with S^{2-} anions and with S^{4+} and S^{6+} cations) separately. Indeed, as could be seen from the reviews on the crystal chemistry of sulfides [25] and sulfates [26], the structural organization principles in these two groups are dramatically different. One would expect that the complexity-generation mechanisms would also be different. S. Krivovichev et al. [44] and S. Krivovichev [67] outlined the following crystal–chemical factors that lead to the origin of high complexity in minerals: (i) the presence in the crystal structure of large polyatomic clusters (sometimes of the nanoscale size) that are thought to exist in natural environments prior to their self-assembly and crystallization of respective minerals; (ii) high hydration state in crystal structures of minerals with complex heteropolyhedral units; (iii) formation of superstructures of otherwise simple structure types; and (iv) multi-modular construction formed as a combination of modules extracted from different archetype structures. In the next sections, we consider the most structurally complex minerals in sulfosalts and sulfides, on the one hand, and in sulfates and sulfites, on the other hand, in order to reveal basic mechanisms governing the formation of complex structures in both groups of minerals.

3.3.1. Sulfides and Sulfosalts

Table 4 provides a list of the ten most structurally complex sulfides and sulfosalts. Among the minerals listed, the only sulfide sensu stricto is djurleite, $Cu_{31}S_{16}$, the mineral usually found in secondary enrichment zones of copper deposits [68,69]. Its crystal structure [70] is monoclinic and is a defect derivative of high-chalcocite. The latter is hexagonal, $P6_3/mmc$, and is based upon hexagonal close packing by S^{2-} anions with interstices filled by Cu atoms. The arrangement of Cu atoms is highly disordered, with occupancies in the range from 0.05 to 0.52, according to the latest crystal structure refinement [71]. The coordination numbers for the Cu sites vary from two (linear coordination) to six (octahedral coordination). In contrast to the crystal structure of high-chalcocite that contains one S site, the crystal structure of djurleite contains 32 independent S positions and 62 fully occupied Cu sites, from which 52 form triangular groups, 9 reside in tetrahedral cavities and 1 has a linear twofold coordination [70]. The recent studies [72] indicated that the situation is probably even more complex, with deficiency observed for some Cu sites and splitting detected for eight Cu sites so that the crystal–chemical formula for the mineral should be written as $Cu_{61.39}S_{32}$. Taking into account the presence of disordered Cu sites, the structural complexity parameters for high-chalcocite are 2.413 bit/atom and 53.088 bit/cell, which can be compared to those of djurleite according to the data reported by Evans [70]:

6.555 bit/atom and 2464.525 bit/cell. Thus, the relation between the total complexity of the superstructure (djurleite) and the substructure (chalcocite) is more than 46 times. The relations between the unit cells of djurleite and chalcocite have been outlined by Evans [70].

With the exception of djurleite, all other minerals listed in Table 4 are sulfosalts. Their extreme and unique complexity has been the subject of a number of reviews, which strongly outline modularity as a basic structure-building principle [73–77]. Indeed, all the sulfosalts mentioned in Table 4 can be described as based upon modules excised from the parent (aristotype) structures of galena, PbS, or its distorted derivative herzenbergite, SnS.

Table 4. Ten most structurally complex sulfosalt minerals and their information-based complexity parameters.

Mineral Name	Chemical Formula	Space Group	v [atoms]	${}^{str}I_G$ [bit/atom]	${}^{str}I_{G,total}$ [bit/cell]	Ref.
Incomsartorite	$Tl_6Pb_{144}As_{246}S_{516}$	$P2_1/n$	924	7.852	7255.016	[78]
Chovanite 8 Å	$Pb_{15-2x}Sb_{14+2x}S_{36}O_x$ (x ~0.2)	$P2_1/c$	524	7.033	3685.514	[79,80]
Meerschautite	$Ag_{12}Pb_{84}Sb_{90}S_{224}O$	$P2_1$	414	7.693	3185.104	[81]
Argentoliveingite	$Ag_{3+x}Pb_{36-2x}As_{51+x}S_{112}$	$P\bar{1}$	400	7.644	3057.542	[82]
Parasterryite	$Ag_2Pb_{10}Sb_7As_5S_{29}$	$P2_1/c$	424	6.728	2852.638	[83]
Sterryite	$CuAg_3Pb_{19}Sb_{22}(As)_2S_{56}$	$P2_1/n$	424	6.728	2852.638	[83]
Djurleite	$Cu_{31}S_{16}$	$P2_1/c$	376	6.555	2464.525	[70]
Hendekasartorite	$Tl_2Pb_{48}As_{82}S_{172}$	$P2_1/c$	304	6.248	1899.370	[84]
Dalnegroite	$Tl_4Pb_2As_{20}S_{34}$	$P1$	240	7.907	1897.654	[85,86]
Cannizzarite	$Pb_8Bi_{10}S_{33}$	$P2_1/m$	236	6.883	1624.304	[87,88]

From the ten minerals in Table 4, three (incomsartorite, hendekasartorite, and argentoleveingite) belong to the sartorite homologous series as defined by Makovicky [73]. The series consists of structures formed by slices of an SnS archetype structure (two atomic layers thick), cut and glide-plane-twinned along the $(301)_{SnS}$ plane [77]. The ribbons cut out from the two-atom-thick SnS slices are either three or four-cation coordination polyhedra wide and are denoted as 3 and 4, respectively. Incomsartorite and hendekasartorite [78,84] belong to the 3:3 combinations of ribbons, i.e., are based upon ribbons of the same width. Together with enneasartorite [89,90] and decatriasartorite [90], these two minerals form the anion-omission derivative (AOD) series. The parent archetype structure for this series is the ideal structure of $PbAs_2S_4$ that was reported by Iitaka and Nowacki [91] as a subcell of "sartorite". The members of the AOD series are obtained by modification of this parent structure through atomic substitutions and omissions discussed in detail in [90]. The complexity parameters for the parent structure are v = 28 atoms; I_G = 2.807 bit/atom; $I_{G,total}$ = 78.606 bit/cell. Thus, the chemical and structural modification of the parent structure in incomsartorite results in the increase of structural information by almost two orders of magnitude. It is important to emphasize that, despite the overall lower complexity of the reduced S minerals relative to the oxidized ones (Table 3), the most complex S mineral is the sulfosalt incomsartorite $Tl_6Pb_{144}As_{246}S_{516}$ with 7255 bit/cell. It should be mentioned, however, that the crystal structure of this mineral is incommensurate (hence the prefix "income"), and the unit-cell parameters reported in the original study by Topa et al. [78] are for the approximant phase (i.e., the crystal structure that "approximates" the atomic structure of the incommensurate phase). The total structural information content for another member of the AOD series, hendekasartorite, $Tl_2Pb_{48}As_{82}S_{172,}$ is 1899.370 bit/cell, which is more than 24 times higher than that for the ideal parent structure.

Argentoliveingite, $Ag_{3+x}Pb_{36-2x}As_{51+x}S_{112}$, is another member of the sartorite homologous series but is not a member of the AOD series based upon 3 ribbons. Instead, in its structure, the alternation of layers of 3 and 4 ribbons is observed with the sequence . . .444343444343. . . consisting of twelve layers stacked along the c parameter of ~138 Å. Topa et al. [82] showed that the structure of argentoliveingite is a superstructure relative to

the imaginary substructure of the hypothetical monoclinic or triclinic "IL" phase with six layers per unit cell and the *c* parameter of ~69 Å. The structural complexity of this parent phase would be at least two times lower than that of argentoliveingite (3057.042 bit/cell), i.e., about 1500 bit/cell. This value would still qualify the "IL" phase as very complex (>1000 bit/cell [41]). Thus, the origin of complexity in argentolivengeite is the result of the combination of two factors: the unusual sequence of structural modules (343444) and the chemical and structural modification that leads to the doubling of the *c* parameter and formation of a superstructure.

Chovanite, $Pb_{15-2x}Sb_{14+2x}S_{36}O_x$ (x ~0.2), is a rare oxysulfosalt originally described from Low Tatra Mountains, Slovakia, by Topa et al. [79]. The mineral was described as monoclinic, $C2/m$, a = 48.189(48), b = 4.1104(40), c = 34.235(35) Å, β = 106.059(15)°, and V = 6517(11) Å^3. The calculation of structural complexity parameters for the original structure model provides v = 132 atoms, I_G = 6.044 bit/atom, and $I_{G,total}$ = 797.860 bit/cell, which characterizes the mineral as structurally complex (500–1000 bit/cell [41]). Later, Biagioni and Moëlo [80] described two new occurrences of chovanite in the Apuan Alps, Italy. In particular, they discovered a variety of chovanite ("chovanite 8 Å") with the doubled *b* parameter and the monoclinic space group $P2_1/c$ (a = 34.052(3), b = 8.2027(7), c = 48.078(4) Å, β = 106.258(4)°, and V = 12891.9(19) Å^3). The doubling of the *b* unit-cell parameter and the change of the unit-cell centering type from *C* to *P* results in the four-times increase of the reduced unit-cell volume and the ~4.6-fold increase of the amount of total structural information to 3685.514 bit/cell. Thus, the high complexity of chovanite 8 Å is a consequence of chemical and structural modification of the original complex structure formed by the combination of three different types of modules identified by Topa et al. [79] as walls, partitions, and boxwork in-fills (see original study for details).

Meerschautite, sterryite, and parasterryite are three very complex minerals (Table 4) that have been considered expanded derivatives of owyheeite, $Ag_3Pb_{10}Sb_{11}S_{28}$ [92]. The crystal structure of the latter mineral was determined by Laufek et al. [93] as a substructure with the 4 Å parameter along the direction of the SnS-like ribbons. The structural model corresponds to an intermediately complex structure with 488.846 bit/cell. The recent re-determination of the crystal structure of owyheeite with the 8 Å parameter [94] resulted in the structure model with 1185.691 bit/cell (more than a twofold increase). The structure models for meerschautite, sterryite, and parasterryite have been determined for the unit cells with ~8 Å parameters, i.e., they all have parent substructures with unit-cell volumes twice as smaller as those reported for real minerals. The transition from the owyheeite structure to the structures of meerschautite, sterryite, and parasterryite corresponds to some complexification of the former by the insertion of additional ribbons ("arms") to the original pseudotrigonal columns [95]. This topological modification (expansion) results in the formation of very complex topologies, which, however, have ~4 Å substructures with at least twice as smaller structural information. Therefore, as in the case of chovanite, the origin of complexity in meerschautite, sterryite, and parasterryite is due to the combination of complex modular arrangements and superstructure resulting from chemical and structural modification of the underlying topology.

The crystal structure of dalnegroite, $Tl_4Pb_2As_{20}S_{34}$, was characterized by Bindi et al. [86] as a "masterpiece of structural complexity". Indeed, with 1897.654 bit/cell, it is the ninth structurally complex sulfosalt known to date. The crystal structure is based upon the slabs of two types, derived from the PbS and SnS archetypes, and is a 1 × 1 × 2 superstructure with respect to chabournéite, $Tl_{2.36}Sb_{5.98}As_{4.59}S_{17}$ [96]. The crystal structure of the latter can be regarded as complex: v = 120 atoms; I_G = 5.907 bit/atom; $I_{G,total}$ = 708.827 bit/cell. The formation of the superstructure is due to some chemical and structural modifications of the already complex substructure and the resulting decrease of symmetry from centrosymmetric to a non-centrosymmetric triclinic group.

Topa et al. [87] suggested considering cannizzarite not as a single mineral but as a variable-fit homologous series of closely related phases. However, at present, the IMA lists cannizzarite as a phase with the well-defined composition $Pb_8Bi_{10}S_{33}$ [28]. The crys-

tal structure of the mineral contains two layers, denoted as Q and H. The Q layers are pseudo-tetragonal and have the (Pb,Bi)(S,Se)$_2$ composition, whereas the H layers are pseudo-hexagonal and have the formula (Pb,Bi)$_2$(S,Se)$_3$. The layers are commensurate in one direction and incommensurate (non-fit) in the perpendicular direction, which results in one extensive unit-cell parameter. There are several phases where the match between the layers is achieved, with the 3H:5Q and 7H:12Q members considered to be terminal [87]. The 3H:5Q notation means that there is a match between the three parameters of the H layer and the five parameters of the Q layer. The structural information of 1624.304 bit/cell reported in Table 4 is observed for the 7H:12Q cannizzarite, for which the crystal-structure data were reported by Topa et al. [87]. The natural 3H:5Q cannizzarite was investigated by Borisov et al. [88] on the material from Kudryaviy volcano, Iturup Island, Kurily Archipelago, Russia. The structural complexity of this mineral is much smaller: v = 50 atoms; I_G = 4.644 bit/atom; $I_{G,total}$ = 232.193 bit/cell. On the other hand, Matzat [97] reported on the crystal structure of synthetic cannizzarite with the formula $Pb_{46}Bi_{54}S_{127}$ with a total structural information of 3553.253 bit/cell and a unit-cell parameter of 189.8 Å. Thus, the high structural complexity of cannizzarite is due to the misfit between two layered modules, which, in some cases, may produce exceptionally large unit cells and, as a consequence, high structural information.

The examples of very complex crystal structures of minerals containing S^{2-} ions considered above indicate that complexity-generating mechanisms in sulfosalts and sulfides involve three basic mechanisms: (a) the complex combination of variable modules produces complex structural arrangements (200–1500 bit/cell); (b) the chemical and structural modifications of already complex structures result in the formation of very complex superstructures; and (c) the misfit between different modules may give rise to the formation of long-range-ordered superstructures (as observed in cannizzarite).

3.3.2. Sulfates

Table 5 provides the list of the 10 most structurally complex sulfate minerals, together with their complexity parameters. The presence of oxygen as one of the principal mineral-forming constituents (in oxysulfosalts, it is of marginal importance since their structures are based upon S-coordinated coordination polyhedra) changes the structure-building principles in a very significant way. Whereas the crystal structures of sulfosalts and oxysulfosalts are based upon the slabs or ribbons excised from parent PbS and/or SnS structure types, the crystal structures of oxysalts have no one or two aristotype structures (if any) but differ essentially in their structural architecture.

The bases of the crystal structures of fantappièite, sacrofanite, and giuseppettite are aluminosilicate frameworks, which belong to the ABC type or the sodalite–cancrinite group [98,99] and are built up from the alternation of sheets formed by six-membered rings of SiO_4 and AlO_4 tetrahedra arranged in different positions denoted as A, B, and C, in the very same way how A, B, and C layers of ideal spheres are arranged in sphere closest packings. The sequence of layers is 11-, 28-, and 33-fold in giuseppettite, sacrofanite, and fantappièite, respectively, which corresponds to the order of the increasing structural complexity [100]. The alternative way to describe the framework construction is in terms of polyhedral secondary building units or cages [41]. The cages within the frameworks are occupied by Na^+, $K^{+,}$ and Ca^{2+} cations, as well as by H_2O and SO_4 groups. Thus, sulfate groups do not participate in the structure architecture but play the subordinate role as cage-filling constituents and charge-compensating agents. The driver for the high structural complexity of the three minerals is the complex modular construction of the aluminosilicate frameworks.

Table 5. Ten most structurally complex sulfate minerals and their information-based complexity parameters.

Mineral Name	Chemical Formula	Space Group	v [at.]	${}^{str}I_G$ [bit/atom]	${}^{str}I_{G,total}$ [bit/cell]	Ref.
Fantappièite	$(Na_{82.5}Ca_{33}K_{16.5})[Al_{99}Si_{99}O_{396}](SO_4)_{33}(H_2O)_6$	$P\bar{3}$	821	7.245	5948.330	[101]
Sacrofanite	$Na_{61}K_{19}Ca_{32}[Si_{84}Al_{84}O_{336}](SO_4)_{26}Cl_2F_6 \cdot 2H_2O$	$P\bar{6}2c$	834	6.376	5317.353	[102]
Voltaite	$K_2Fe_5Fe_4Al(SO_4)_{12} \cdot 18H_2O$	$Fd\bar{3}c$	764	4.160	3177.944	[103]
Putnisite	$SrCa_4Cr_8(CO_3)_8(SO_4)(OH)_{16} \cdot 25H_2O$	$Pnma$	488	6.078	2966.200	[104]
Giuseppettite	$Na_{42}K_{16}Ca_6(Si_{48}Al_{48}O_{192})(SO_4)_{10}Cl_2(H_2O)_5$	$P31c$	430	6.333	2723.097	[105]
Vonbezingite	$Ca_6Cu_3(SO_4)_3(OH)_{12} \cdot 2H_2O$	$P2_1/c$	400	6.644	2657.542	[106]
Natrozippeite	$Na_5(UO_2)_8(SO_4)_4O_5(OH)_3 \cdot 12H_2O$	$P2_1/n$	384	6.585	2528.626	[107]
Apjohnite	$MnAl_2(SO_4)_4 \cdot 22H_2O$	$P2_1/c$	356	6.476	2305.361	[108]
Sejkoraite-(Y)	$Y(UO_2)_4O_3(SO_4)_2(OH) \cdot 13H_2O$	$P\bar{1}$	264	7.044	1859.720	[109]
Ramazzoite	$[Mg_8Cu_{12}(PO_4)(CO_3)_4(OH)_{24}](HSO_4)(SO_4)_2 \cdot 56H_2O$	$P\bar{4}3m$	400	4.620	1848.162	[110]

The same subordinate role is adopted by sulfate groups in the crystal structures of putnisite and ramazzoite, which are both based on polyoxometalate units of different sizes and topologies [111]. The crystal structure of putnisite contains a wheel-shaped flat $[Cr^{3+}{}_8(OH)_{16}(CO_3)_8]^{8-}$ anion surrounded by Ca^{2+} and Sr^{2+} cations, $(SO_4)^{2-}$ groups and H_2O molecules [104]. The topological complexity of the cluster is rather low (141 bit/cluster), and it is remarkable that its symmetry is non-crystallographic and corresponds to the symmetry group $\bar{8}2m$. In the crystal structure, the ideal symmetry is decreased to m, which results in the increasing complexity of 277 bit/cluster, and the reduced unit cell contains four such clusters. The crystal structure of ramazzoite consists of the $[Mg_8Cu_{12}(PO_4)(CO_3)_4(OH)_{24}(H_2O)_{20}]^{5+}$ polycation based upon the $\{PCu_{12}O_{40}\}$ α-Keggin cluster formed by a central (PO_4) tetrahedron and twelve CuO_6 octahedra [110]. The cuprophosphate core is surrounded by MgO_6 octahedra and disordered CO_3 groups that complete the cluster architecture. The resulting cluster is rather complex (370 bit/cluster). The $(SO_4)^{2-}$ and $(HSO_4)^-$ groups, together with 56 H_2O molecules per formula unit, provide the linkage of the clusters via a complex system of hydrogen bonding. The high complexity of putnisite and ramazzoite is the result of the combination of three complexity-generating factors: the presence of polyatomic clusters, their packing within the reduced unit cell, and the high hydration state.

Figure 3 illustrates contributions of various factors to the overall structural complexity of ramazzoite (**Rmz**), putnisite (**Pni**), sejkoraite-(Y) (**Sej-Y**), natrozippeite (**Nzip**), voltaite (**Vlt**), apjohnite (**Apj**), and vonbezingite (**Vbz**) using ladder diagrams introduced in [112] (the mineral symbols follow the IMA recommendations [113]). The following factors are recognized: topological complexity or topological information (TI; the information of the basic structural unit in its ideal (maximal) symmetry group); structural complexity or structural information (SI) emerging as a result of a possible symmetry breaking when cluster is enclosed into the real crystal structure; unit stacking (US) is additional information that originates if there is more than one symmetrically independent basic structural unit; information due to interstitial ions and groups (IS = interstitial structure) with the exception of H atoms; information due to the H atoms (HB = hydrogen bonding). For instance, it could be seen that the contribution from H atoms in the crystal structure of ramazzoite is higher than 50% of all information the structure contains.

Sejkoraite-(Y) and natrozippeite are both members of the zippeite group of hydrated uranyl sulfates [107]. Both structures are based upon the same uranyl sulfate layers with a rather simple topology (72 bit/cell), but the presence of interlayer cations and H_2O groups results in symmetry breaking (formation of layer superstructure relative the ideal symmetry), which contributes additional 521 and 593 bit to the structural complexity of the layers, respectively (about 28 and 23% of the total complexity, respectively). The contributions of H atoms are also considerable and constitute 45 and 34% of the total complexity for sejkoraite-(Y) and natrozippeite, respectively.

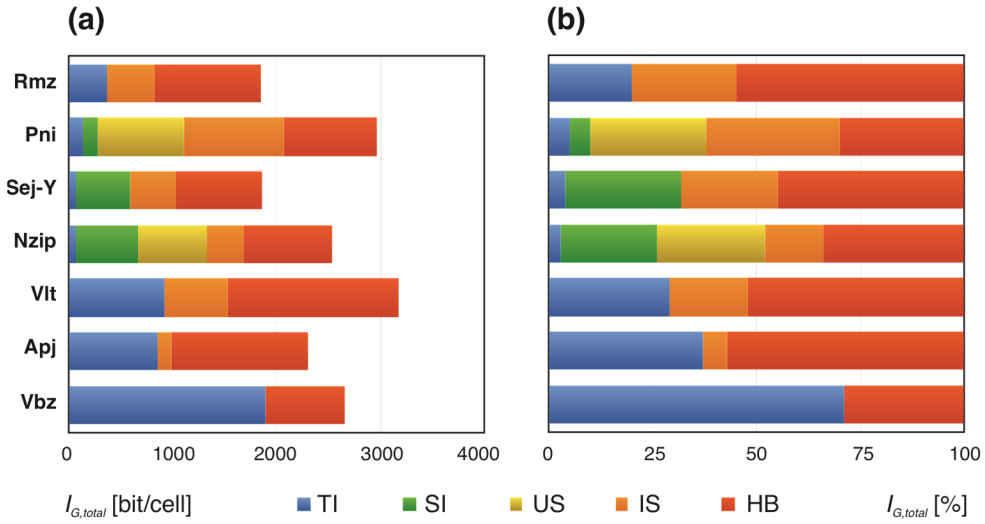


Figure 3. Ladder diagrams (in bit/cell (**a**) and in%/cell (**b**)) showing the absolute (**a**) and relative (**b**) contributions of different factors to the structural complexity of ramazzoite (**Rmz**), putnisite (**Pni**), sejkoraite-(Y) (**Sej-Y**), natrozippeite (**Nzip**), voltaite (**Vlt**), apjohnite (**Apj**), and vonbezingite (**Vbz**). Legend: TI = topological information; SI = structural information; US = unit stacking; IS = interstitial structure; HB = hydrogen bonding.

The crystal structure of voltaite and voltaite-group minerals [103,114–118] (only one representative is given in Table 5, whereas the complexities of all the members of the group are of the same order) is based upon a complex (921 bit/cell) framework of Fe-centered octahedra and SO_4 tetrahedra linked by sharing common O atoms. The contribution of the H atoms exceeds 50%, highlighting the dominating role of the hydration state in the high complexity of the mineral.

Apjohnite is given as a representative of the halotrichite group of minerals [108,119]. Its crystal structure contains two symmetrically independent $Al(H_2O)_6$ octahedra, one symmetrically independent cluster $Mn(H_2O)_5(SO_4)$, three symmetrically independent SO_4 tetrahedra, and five additional H_2O sites. The structural integrity, through hydrogen bonding only, accounts for ~57% of the total complexity. Thus, the high complexity of apjohnite is the result of the diversity of structural elements and the high hydration state.

Vonbezingite can be considered an enigma among the minerals listed in Table 5 since the contribution of H atoms to its complexity is the smallest (about 29%); meanwhile, it does not contain obvious structural units of high complexity. The crystal structure consists of 12 Ca and 6 Cu sites, as well as 6 independent SO_4 tetrahedra. Dai and Harlow [106] indicated the existence of the substructure with the *b*-parameter halved and the space group changing from $P2_1/c$ to $C2/c$, which means that the reduced subcell is four times smaller than that of the real structure, leading to the decreased structural information of ~800 bit/cell. The substructure differs from the real structure by the disorder of sulfate tetrahedra (Dai and Harlow [106] pointed out the possibility that the subcell corresponds to a high-temperature polymorph of vonbezingite). Thus, the high complexity of vonbezingite is the result of structure ordering accompanied by superstructure formation.

The very complex sulfate minerals considered in this section exhibit several complexity-generating mechanisms: (i) complex modular construction (fantappièite, sacrofanite, and giuseppettite), but with a subordinate role of sulfate groups; (ii) the presence of polyatomic clusters with complex packing within a unit cell (ramazzoite, putnisite), but, again, with a subordinate role of sulfate groups; (iii) superstructure formation (sejkoraite-(Y), natrozippeite, vonbezingite); (iv) framework complexity (voltaite and voltaite-group minerals) (probably relates to (i), but needs a detailed topological analysis); (v) diversity of structural units (apjohnite and halotrichite-group minerals); and (vi) high hydration state (all minerals). The hydration state is invariably very important for the minerals listed in Table 5, never

lower than 29% and reaching up to 57% (in apjohnite), reflecting near-surface crystallization from aqueous solutions under relatively low-temperature and low-pressure conditions.

3.4. Evolution of the Chemical and Structural Complexity of S Minerals

The evolution of chemical and structural complexities through geological time can be investigated using the lists of mineral species existing at different evolutionary eons provided in [120,121]. The results are given in Table 6 and are illustrated in Figure 4. Both the chemical and structural complexity of S minerals increased in geological time in terms of both atomic and total information amounts. The starting point of mineral evolution is that of the "presolar ur-minerals", the earliest mineral phases to appear in the presolar nebulae (I). Chondritic meteorites incorporate about 10 primary sulfides and 1 sulfate (II). For the Hadean Eon, 77 sulfides and 20 sulfates were estimated by Hazen [121] (III), whereas post-Hadean processes were responsible for the appearance of 510 sulfides and 531 sulfates known today (IV).

Table 6. Chemical and structural complexities of sulfur minerals for the four stages of mineral evolution (I–IV).

Stages	m_i	$^{chem}I_G$ [bit/atom]		$^{chem}I_{G,total}$ [bit/f.u.]		m_i	$^{str}I_G$ [bit/atom]		$^{str}I_{G,total}$ [bit/cell]	
		$\overline{X}$	$\sigma_{\overline{X}}$	$\overline{X}$	$\sigma_{\overline{X}}$		$\overline{X}$	$\sigma_{\overline{X}}$	$\overline{X}$	$\sigma_{\overline{X}}$
Sulfides and sulfosalts										
I	3	1	0	2	0	3	1.24	0.24	15.17	13.17
II	10	1.04	0.05	5.27	1.83	10	1.70	0.42	52.63	41.67
III	77	1.28	0.04	17.27	4.17	77	2.21	0.16	142.99	44.87
IV	529	1.47	0.01	38.68	2.68	291	2.74	0.08	290.86	17.05
Sulfates and sulfites										
I	0	-	-	-	-	0	-	-	-	-
II	1	1.25	1	7.51		1	1.25		22.530	
III	20	1.54	0.05	36.73	5.26	20	3.57	0.31	294.47	60.13
IV	589	1.69	0.01	47.46	3.69	273	3.68	0.07	329.80	19.89

m_i = number of minerals taken into account; $\overline{X}$ = arithmetic mean; $\sigma_{\overline{X}}$ = standard error of arithmetic mean.

The formation of most structurally complex S minerals agrees well with their formation in relatively late geological times. For instance, the sartorite-group minerals, from which incomsartorite is the most complex sulfur mineral known so far, are typical for the Lengenbach deposit, Binn Valley, and Swiss Alps. Hofmann and Knill [122] pointed out that the formation of the unique Lengenbach sulfosalt mineralogy is due to an isochemical Alpine metamorphism. The isotopic composition of sulfur (namely, the enrichment in light isotopes) indicates that the primary stratiform sulfide deposit was formed near or at the bottom of the sea due to the activity of sulfate-reducing bacteria. According to Hofmann and Knill [122], during Alpine metamorphism, the primary sulfide ore minerals recrystallized and released Tl, As, and Sb to form a Pb-As-Tl-Sb-rich sulfide melt, which underwent crystallization under slow cooling conditions to result in the formation of a unique assemblage of sulfides and sulfosalts. The metamorphic facies correspond to greenschist or low amphibolite grade conditions (~500 °C). Thus, the formation of most complex S minerals is related to relatively recent (<60 Ma) geological processes and was originally involved with bacterial activity, i.e., with life as a phenomenon of nature.

The origin of most structurally complex sulfate minerals, fantappièite and sacrofanite (as well as giuseppettite), is connected with the Sabatini volcanic complex that was active between 0.5 and 0.09 Ma ago [123]. The formation of other sulfates listed in Table 5 is related to oxidation zones of sulfide or uraninite mineral deposits, including mineral crystallization in abandoned mines and/or from surface and groundwater. For instance, halotrichite-group minerals currently form in the geothermal fields of modern volcanos such as the Koshelevsky and Centralny Semyachik volcanos (Kamchatka peninsula, Russia) [119].

Gendrin et al. [4] pointed out the spectroscopic evidence of the occurrence of halotrichite-group minerals on the surface of Mars. Taking into account the scarcity of knowledge about Mars mineralogy, halotrichite is presently the most complex mineral known to be present on Mars.

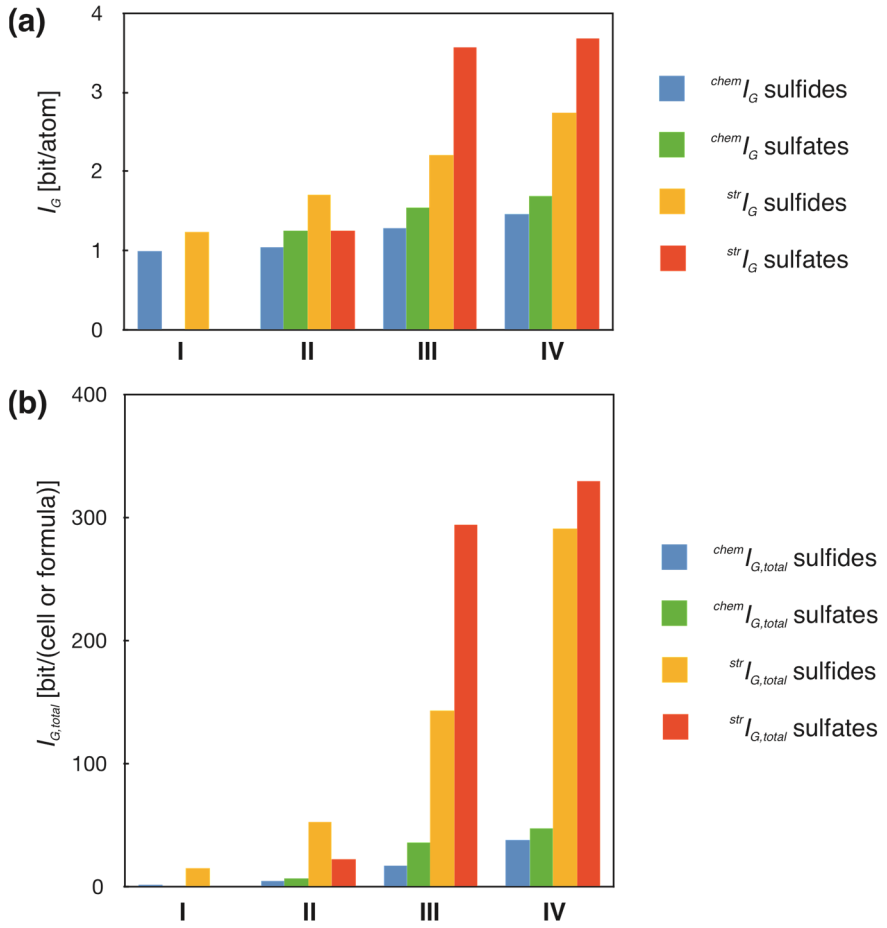


Figure 4. Evolution of atomic (**a**) and total (**b**) structural information versus four eons of mineral evolution (I–IV). See text for details.

4. Conclusions

The features of chemical and structural complexities of sulfur minerals follow the general trend observed for all minerals [65] and selenium [50] and tellurium [51] minerals: (a) there is a positive and statistically significant correlation between information-based chemical and structural complexity parameters, on one hand, and the number of species-defining chemical elements (*N*), on the other; (b) chemical and structural complexity correlate, so that, on average, the increase of chemical information results in the increase of structural information; (c) both chemical and structural complexity parameters increase with the passage of geological time. Similarly to selenium and tellurium minerals, there are two groups of sulfur minerals: those containing S in reduced forms (mostly S^{2-}) and those containing S^{4+} and S^{6+} ions. The first group is, on average, more chemically and structurally simpler than the second group. However, the most structurally complex sulfur mineral is incomsartorite, which is a sulfosalt. The complexity-generating mechanisms in the two groups of S minerals are different as well. In sulfides and especially in sulfosalts, the leading mechanisms are the formation of complex modular architectures (involving different modules arranged in a complex fashion), which are further complexified through chemical substitutions to form superstructures of high complexity. The drivers for structural complexity in sulfates are much more diverse and, along with those present in sulfosalts,

also include the formation of polyatomic clusters and high hydration states that, in some cases, causes the doubling of structural information.

It has recently been shown [124,125] that simpler minerals are usually older and have high thermodynamic stability (in particular, higher melting temperatures) compared to the more complex minerals. It seems that the same is also true for the mineral abundances: rock-forming sulfides (e.g., galena, pyrite, sphalerite, etc.) and sulfates (e.g., baryte, anhydrite, gypsum) are usually very simple (0–20 bit/cell) or simple (20–100 bit/cell), whereas complex and very complex species are usually rare.

Author Contributions: Conceptualization, V.G.K. and S.V.K.; methodology, V.G.K. and S.V.K.; formal analysis, V.G.K., S.V.K. and G.L.S.; investigation, V.G.K., S.V.K. and G.L.S.; writing—original draft preparation, V.G.K. and S.V.K.; writing—review and editing, V.G.K. and S.V.K.; visualization, V.G.K. and S.V.K.; funding acquisition, S.V.K. All authors have read and agreed to the published version of the manuscript.

Funding: This research was funded by the Russian Science Foundation, grant 19-17-00038.

Data Availability Statement: The data on the structural and chemical complexity parameters of S minerals are available from the authors upon request.

Acknowledgments: We are grateful to Dan Topa (Naturhistorisches Museum Wien) for sharing the data on the crystal structure of incomsartorite prior to publication.

Conflicts of Interest: The authors declare no conflict of interest.

References

1. Brimblecombe, P. 10.14—The Global Sulfur Cycle. In *Treatise on Geochemistry*, 2nd ed.; Holland, H.D., Turekian, K.K., Eds.; Elsevier: Oxford, UK, 2014; pp. 559–591, ISBN 978-0-08-098300-4.
2. Wedepohl, H.K. The Composition of the Continental Crust. *Geochim. Cosmochim. Acta* **1995**, *59*, 1217–1232. [CrossRef]
3. Vaughan, D.J. Sulfide Mineralogy and Geochemistry: Introduction and Overview. *Rev. Miner. Geochem.* **2006**, *61*, 1–5. [CrossRef]
4. Gendrin, A.; Mangold, N.; Bibring, J.-P.; Langevin, Y.; Gondet, B.; Poulet, F.; Bonello, G.; Quantin, C.; Mustard, J.; Arvidson, R.; et al. Sulfates in Martian Layered Terrains: The OMEGA/Mars Express View. *Science* **2005**, *307*, 1587–1591. [CrossRef]
5. Langevin, Y.; Poulet, F.; Bibring, J.-P.; Gondet, B. Sulfates in the North Polar Region of Mars Detected by OMEGA/Mars Express. *Science* **2005**, *307*, 1584–1586. [CrossRef]
6. Wendt, L.; Gross, C.; Kneissl, T.; Sowe, M.; Combe, J.-P.; LeDeit, L.; McGuire, P.C.; Neukum, G. Sulfates and Iron Oxides in Ophir Chasma, Mars, Based on OMEGA and CRISM Observations. *Icarus* **2011**, *213*, 86–103. [CrossRef]
7. Majzlan, J.; Alpers, C.N.; Koch, C.B.; McCleskey, R.B.; Myneni, S.C.B.; Neil, J.M. Vibrational, X-ray Absorption, and Mössbauer Spectra of Sulfate Minerals from the Weathered Massive Sulfide Deposit at Iron Mountain, California. *Chem. Geol.* **2011**, *284*, 296–305. [CrossRef]
8. Wilson, S.; Bish, D.L. Stability of Mg-Sulfate Minerals in the Presence of Smectites: Possible Mineralogical Controls on H_2O Cycling and Biomarker Preservation on Mars. *Geochim. Cosmochim. Acta* **2012**, *96*, 120–133. [CrossRef]
9. Kong, W.G.; Wang, A.; Chou, I.-M. Experimental Determination of the Phase Boundary between Kornelite and Pentahydrated Ferric Sulfate at 0.1 MPa. *Chem. Geol.* **2011**, *284*, 333–338. [CrossRef]
10. Norlund, K.L.I.; Baron, C.; Warren, L.A. Jarosite Formation by an AMD Sulphide-Oxidizing Environmental Enrichment: Implications for Biomarkers on Mars. *Chem. Geol.* **2010**, *275*, 235–242. [CrossRef]
11. Marion, G.M.; Catling, D.C.; Kargel, J.S.; Crowley, J.K. Modeling Calcium Sulfate Chemistries with Applications to Mars. *Icarus* **2016**, *278*, 31–37. [CrossRef]
12. Cao, H.; Chen, J.; Ling, Z. Laboratory Synthesis and Spectroscopic Studies of Hydrated Al-Sulfates Relevant to Mars. *Icarus* **2019**, *333*, 283–293. [CrossRef]
13. Paramanick, S.; Rajesh, V.J.; Praveen, M.N.; Sajinkumar, K.S.; Bhattacharya, S. Spectral and Chemical Characterization of Copiapite and Rozenite from Padinjarathara in Wayanad, Southern India: Implications for Mars Exploration. *Chem. Geol.* **2021**, *575*, 120043. [CrossRef]
14. Sheppard, R.Y.; Thorpe, M.T.; Fraeman, A.A.; Fox, V.K.; Milliken, R.E. Merging Perspectives on Secondary Minerals on Mars: A Review of Ancient Water-Rock Interactions in Gale Crater Inferred from Orbital and In-Situ Observations. *Minerals* **2021**, *11*, 986. [CrossRef]
15. Suga, H.; Suzuki, K.; Usui, T.; Yamaguchi, A.; Sekizawa, O.; Nitta, K.; Takeichi, Y.; Ohigashi, T.; Takahashi, Y. A New Constraint on the Physicochemical Condition of Mars Surface during the Amazonian Epoch Based on Chemical Speciation for Secondary Minerals in Martian Nakhlites. *Minerals* **2021**, *11*, 514. [CrossRef]
16. Szynkiewicz, A.; Bishop, J.L. Assessment of Sulfate Sources under Cold Conditions as a Geochemical Proxy for the Origin of Sulfates in the Circumpolar Dunes on Mars. *Minerals* **2021**, *11*, 507. [CrossRef]

17. Grasby, S.E.; Percival, J.B.; Bilot, I.; Ardakani, O.H.; Smith, I.R.; Galloway, J.; Bringué, M.; McLoughlin-Coleman, T. Extensive Jarosite Deposits Formed through Auto-Combustion and Weathering of Pyritiferous Mudstone, Smoking Hills (Ingniryuat), Northwest Territories, Canadian Arctic—A Potential Mars Analogue. *Chem. Geol.* **2022**, *587*, 120634. [CrossRef]
18. Wildner, M.; Zakharov, B.A.; Bogdanov, N.E.; Talla, D.; Boldyreva, E.V.; Miletich, R. Crystallography Relevant to Mars and Galilean Icy Moons: Crystal Behavior of Kieserite-Type Monohydrate Sulfates at Extraterrestrial Conditions down to 15 K. *IUCrJ* **2022**, *9*, 194–203. [CrossRef]
19. Sheppard, R.Y.; Milliken, R.E.; Robertson, K.M. Presence of Clay Minerals Can Obscure Spectral Evidence of Mg Sulfates: Implications for Orbital Observations of Mars. *Icarus* **2022**, *383*, 115083. [CrossRef]
20. Ju, E.; Shi, E.; Xin, Y.; Cao, H.; Liu, C.; Liu, P.; Chen, J.; Fu, X.; Ling, Z. Laboratory Synthesis, Spectroscopic Characteristics, and Conversion Relationships of Five Calcium Sulfate Double Salts Relevant to Mars. *Icarus* **2023**, *401*, 115610. [CrossRef]
21. He, M.; Yan, C.; Li, J.; Suryawanshi, M.P.; Kim, J.; Green, M.A.; Hao, X. Kesterite Solar Cells: Insights into Current Strategies and Challenges. *Adv. Sci.* **2021**, *8*, 2004313. [CrossRef]
22. Wang, A.; He, M.; Green, M.A.; Sun, K.; Hao, X. A Critical Review on the Progress of Kesterite Solar Cells: Current Strategies and Insights. *Adv. Energy Mater.* **2023**, *13*, 2203046. [CrossRef]
23. Vaughan, D. (Ed.) Sulfide Mineralogy and Geochemistry. In *Reviews in Mineralogy and Geochemistry*; Mineralogical Society of America: Washington, DC, USA, 2006; Volume 61.
24. Alpers, C.L.; Jambor, J.L.; Nordstron, D.K. (Eds.) Sulfate Minerals: Crystallography, Geochemistry, and Environmental Significance. In *Reviews in Mineralogy and Geochemistry*; Mineralogical Society of America: Washington, DC, USA, 2000; Volume 40.
25. Makovicky, E. Crystal Structures of Sulfides and Other Chalcogenides. *Rev. Mineral. Geochem.* **2006**, *61*, 7–125. [CrossRef]
26. Hawthorne, F.C.; Krivovichev, S.V.; Burns, P.C. The Crystal Chemistry of Sulfate Minerals. *Rev. Mineral. Geochem.* **2000**, *40*, 1–112. [CrossRef]
27. Christy, A.G. Anomalous mineralogical diversity in the Periodic Table, and its causes. *Miner. Mag.* **2015**, *79*, 33–49. [CrossRef]
28. Pasero, M. The IMA List of Minerals. 2023. Available online: http://cnmnc.units.it (accessed on 11 July 2023).
29. Charykova, M.V.; Krivovichev, V.G. Mineral systems and the thermodynamics of selenites and selenates in the oxidation zone of sulfide ores—A review. *Mineral. Petrol.* **2017**, *111*, 121–134. [CrossRef]
30. Krivovichev, V.G.; Charykova, M.V.; Vishnevsky, A.V. The thermodynamics of selenium minerals in near-surface environments. *Minerals* **2017**, *7*, 188. [CrossRef]
31. Morrison, S.M.; Runyon, S.E.; Hazen, R.M. The Paleomineralogy of the Hadean Eon Revisited. *Life* **2018**, *8*, 64. [CrossRef]
32. Hazen, R.M.; Morrison, S.M. An Evolutionary System of Mineralogy. Part I: Stellar Mineralogy (>13 to 4.6 Ga). *Am. Miner.* **2020**, *105*, 627–651. [CrossRef]
33. Morrison, S.M.; Hazen, R.M. An Evolutionary System of Mineralogy. Part II: Interstellar and Solar Nebula Primary Condensation Mineralogy (>4.565 Ga). *Am. Miner.* **2020**, *105*, 1508–1535. [CrossRef]
34. Hazen, R.M.; Morrison, S.M.; Prabhu, A. An Evolutionary System of Mineralogy. Part III: Primary Chondrule Mineralogy (4566 to 4561 Ma). *Am. Miner.* **2021**, *106*, 325–350. [CrossRef]
35. Morrison, S.M.; Hazen, R.M. An Evolutionary System of Mineralogy, Part IV: Planetesimal Differentiation and Impact Mineralization (4566 to 4560 Ma). *Am. Miner.* **2021**, *106*, 730–761. [CrossRef]
36. Hazen, R.M.; Morrison, S.M. An Evolutionary System of Mineralogy, Part V: Aqueous and Thermal Alteration of Planetesimals (Similar to 4565 to 4550 Ma). *Am. Miner.* **2021**, *106*, 1388–1419. [CrossRef]
37. Morrison, S.M.; Prabhu, A.; Hazen, R.M. An Evolutionary System of Mineralogy, Part VI: Earth's Earliest Hadean Crust (>4370 Ma). *Am. Miner.* **2023**, *108*, 42–58. [CrossRef]
38. Hazen, R.M.; Morrison, S.M. On the Paragenetic Modes of Minerals: A Mineral Evolution Perspective. *Am. Miner.* **2022**, *107*, 1262–1287. [CrossRef]
39. Hazen, R.M.; Morrison, S.M.; Krivovichev, S.V.; Downs, R.T. Lumping and Splitting: Toward a Classification of Mineral Natural Kinds. *Am. Miner.* **2022**, *107*, 1288–1301. [CrossRef]
40. Krivovichev, S.V. Topological Complexity of Crystal Structures: Quantitative Approach. *Acta Crystallogr.* **2012**, *A68*, 393–398. [CrossRef]
41. Krivovichev, S.V. Structural Complexity of Minerals: Information Storage and Processing in the Mineral World. *Miner. Mag.* **2013**, *77*, 275–326. [CrossRef]
42. Krivovichev, S.V. Which Inorganic Structures Are the Most Complex? *Angew. Chem. Int. Ed.* **2014**, *53*, 654–661. [CrossRef]
43. Krivovichev, S.V. Structural Complexity and Configurational Entropy of Crystals. *Acta Crystallogr.* **2016**, *B72*, 274–276. [CrossRef]
44. Krivovichev, S.V.; Krivovichev, V.G.; Hazen, R.M.; Aksenov, S.M.; Avdontceva, M.S.; Banaru, A.M.; Gorelova, L.A.; Ismagilova, R.M.; Kornyakov, I.V.; Kuporev, I.V.; et al. Structural and Chemical Complexity of Minerals: An Update. *Miner. Mag.* **2022**, *86*, 183–204. [CrossRef]
45. Hazen, R.M.; Downs, R.T.; Eleish, A.; Fox, P.; Gagne, O.C.; Golden, J.J.; Grew, E.S.; Hummer, D.R.; Hystad, G.; Krivovichev, S.V.; et al. Data-Driven Discovery in Mineralogy: Recent Advances in Data Resources, Analysis, and Visualization. *Engineering* **2019**, *5*, 397–405. [CrossRef]
46. Prabhu, A.; Morrison, S.M.; Eleish, A.; Zhong, H.; Huang, F.; Golden, J.J.; Perry, S.N.; Hummer, D.R.; Ralph, J.; Runyon, S.E.; et al. Global Earth Mineral Inventory: A Data Legacy. *Geosci. Data J.* **2021**, *8*, 74–89. [CrossRef]

47. Wang, C.; Hazen, R.M.; Cheng, Q.; Stephenson, M.H.; Zhou, C.; Fox, P.; Shen, S.; Oberhansli, R.; Hou, Z.; Ma, X.; et al. The Deep-Time Digital Earth Program: Data-Driven Discovery in Geosciences. *Natl. Sci. Rev.* **2021**, *8*, nwab027. [CrossRef]
48. Grew, E.S.; Krivovichev, S.V.; Hazen, R.M.; Hystad, G. Evolution of Structural Complexity in Boron Minerals. *Can. Miner.* **2016**, *54*, 125–143. [CrossRef]
49. Grew, E.S.; Hystad, G.; Hazen, R.M.; Krivovichev, S.V.; Gorelova, L.A. How Many Boron Minerals Occur in Earth's Upper Crust? *Am. Miner.* **2017**, *102*, 1573–1587. [CrossRef]
50. Krivovichev, V.G.; Krivovichev, S.V.; Charykova, M.V. Selenium Minerals: Structural and Chemical Diversity and Complexity. *Minerals* **2019**, *9*, 455. [CrossRef]
51. Krivovichev, V.G.; Krivovichev, S.V.; Charykova, M.V. Tellurium Minerals: Structural and Chemical Diversity and Complexity. *Minerals* **2020**, *10*, 623. [CrossRef]
52. Krivovichev, V.G.; Charykova, M.V. *Classification of Mineral Systems*; St. Petersburg University Press: Saint Petersburg, Russia, 2013; 196p. (In Russian)
53. Krivovichev, V.G.; Charykova, M.V. Number of Minerals of Various Chemical elements: Statistics 2012 (a New Approach to an Old Problem). *Zap. Ross. Mineral. Obs.* **2013**, *142*, 36–42. (In Russian; English translation: Geol. Ore Depos. **2014**, *56*, 553–559) [CrossRef]
54. Mandarino, J.A.; Nickel, E.H.; Cesbron, F. Rules of procedure of the Commission on New Minerals and Mineral Names, International Mineralogical Association. *Can. Miner.* **1984**, *22*, 367–368. [CrossRef]
55. Nickel, E.H. The definition of a mineral. *Can. Miner.* **1995**, *33*, 689–690.
56. Nickel, E.H.; Grice, J.D. The IMA Commission on New Minerals and Mineral Names: Procedures and Guidelines on Mineral Nomenclature. *Can. Miner.* **1998**, *36*, 91–926.
57. Nickel, E.H.; Mandarino, J.A. Procedures involving the IMA Commission on New Minerals and Mineral Names and guidelines on mineral nomenclature. *Am. Miner.* **1987**, *72*, 1031–1042.
58. Hawthorne, F.C. The use of end-member charge-arrangements in defining new mineral species and heterovalent substitutions in complex minerals. *Can. Miner.* **2002**, *40*, 699–710. [CrossRef]
59. Hatert, F.; Burke, E.A.J. The IMA-CNMNC dominant-constituent rule revised and extended. *Can. Miner.* **2008**, *46*, 717–728. [CrossRef]
60. Bulakh, A.G.; Zolotarev, A.A.; Krivovichev, V.G. *Structures, Isomorphism, Formulae, Classification of Minerals*; St. Petersburg University Press: Saint Petersburg, Russia, 2014; 133p. (In Russian)
61. Krivovichev, V.G. *Mineral Species*; St. Petersburg University Press: Saint Petersburg, Russia, 2021; 601p. (In Russian)
62. Krivovichev, V.G.; Charykova, M.V.; Krivovichev, S.V. The concept of mineral systems and its application to the study of mineral diversity and evolution. *Eur. J. Mineral.* **2018**, *30*, 219–230. [CrossRef]
63. Pankova, Y.A.; Gorelova, L.A.; Krivovichev, S.V.; Pekov, I.V. The crystal structure of ginorite, $Ca_2[B_{14}O_{20}(OH)_6](H_2O)_5$, and the analysis of dimensional reduction and structural complexity in the CaO-B_2O_3-H_2O system. *Eur. J. Mineral.* **2018**, *30*, 277–287. [CrossRef]
64. Blatov, V.A.; Shevchenko, A.P.; Proserpio, D.M. Applied topological analysis of crystal structures with the program package ToposPro. *Cryst. Growth Des.* **2014**, *14*, 3576–3586. [CrossRef]
65. Krivovichev, S.V.; Krivovichev, V.G.; Hazen, R.M. Structural and chemical complexity of minerals: Correlations and time evolution. *Eur. J. Mineral.* **2018**, *30*, 231–236. [CrossRef]
66. Wall, F.J. *Statistical Data Analysis Handbook*; McGraw-Hill Inc.: New York, NY, USA, 1986; 546p.
67. Krivovichev, S.V. Structural and Chemical Complexity of Minerals: The Information-Based Approach. In *Celebrating the International Year of Mineralogy: Progress and Landmark Discoveries of the Last Decades*; Bindi, L., Cruciani, G., Eds.; Springer Nature: Cham, Switzerland, 2023; pp. 101–129, ISBN 978-3-031-28805-0.
68. Morimoto, N. Djurleite, a new copper sulfide mineral. *Mineral. J.* **1962**, *3*, 338–344. [CrossRef]
69. Szopa, K.; Krzykawski, T.; Banasik, K.; Król, P.; Skreczko, S.; Mounteanou, S.A.; Koziarska, M. EMPA, XRD, and Raman Characterization of Ag-Bearing Djurleite from the Lubin Mine, Lower Silesia, Poland. *Minerals* **2021**, *11*, 454. [CrossRef]
70. Evans, H. Crystal structures of low chalcocite and djurleite. *Z. Kristallogr.* **1979**, *150*, 299–320. [CrossRef]
71. Will, G.; Hinze, E.; Abdelrahman, A.R.M. Crystal Structure Analysis and Refinement of Digenite, $Cu_{1.8}S$, in the Temperature Range 20 to 500 °C under Controlled Sulfur Partial Pressure. *Eur. J. Miner.* **2002**, *14*, 591–598. [CrossRef]
72. Zhou, Y.; Fan, C.; Wen, B.; Zhang, L. Natural djurleite with refined composition $Cu_{61.39}S_{32}$ revealing disorder of some Cu sites. *IUCrData* **2022**, *7*, x220694. [CrossRef]
73. Makovicky, E. The building principles and classification of bismuth-lead sulphosalts and related compounds. *Fortschr. Miner.* **1981**, *59*, 137–190.
74. Makovicky, E. Modular crystal chemistry of sulphosalts and other complex sulphides. *EMU Notes Miner.* **1997**, *1*, 237–271.
75. Makovicky, E. Modularity—Different types and approaches. *EMU Notes Miner.* **1997**, *1*, 315–343.
76. Ferraris, G.; Makovicky, E.; Merlino, S. Crystallography of Modular Materials. In *IUCr Monographs in Crystallography*; Oxford University Press: Oxford, UK, 2004.
77. Makovicky, E. Modular Crystal Chemistry of Thallium Sulfosalts. *Minerals* **2018**, *8*, 478. [CrossRef]
78. Topa, D.; Stoeger, B.; Makovicky, E.; Stanley, C. Incomsartorite, IMA 2016-035. CNMNC Newsletter No. 33, October 2016. *Miner. Mag.* **2016**, *80*, 1136.

79. Topa, D.; Sejkora, J.; Makovicky, E.; Prsek, J.; Ozdin, D.; Putz, H.; Dittrich, H.; Karup-Moller, S. Chovanite, $Pb_{15-2x}Sb_{14+2x}S_{36}O_x$ (x ~ 0.2), a New Sulphosalt Species from the Low Tatra Mountains, Western Carpathians, Slovakia. *Eur. J. Miner.* **2012**, *24*, 727–740. [CrossRef]
80. Biagioni, C.; Moelo, Y. Lead-Antimony Sulfosalts from Tuscany (Italy). XIX. Crystal Chemistry of Chovanite from Two New Occurrences in the Apuan Alps and Its 8 Angstrom Crystal Structure. *Miner. Mag.* **2017**, *81*, 811–831. [CrossRef]
81. Biagioni, C.; Moelo, Y.; Orlandi, P.; Stanley, C.J. Lead-Antimony Sulfosalts from Tuscany (Italy). XVII. Meerschautite, $(Ag,Cu)_{5.5}Pb_{42.4}(Sb,As)_{45.1}S_{112}O_{0.8}$, a New Expanded Derivative of Owyheeite from the Pollone Mine, Valdicastello Carducci: Occurrence and Crystal Structure. *Miner. Mag.* **2016**, *80*, 675–690. [CrossRef]
82. Topa, D.; Kolitsch, U.W.E.; Graeser, S.; Makovicky, E.; Stanley, C. Argentoliveingite, $Ag_{3+x}Pb_{36-2x}As_{51+x}S_{112}$ (0 <= x < 0.5), a New Homeotype of Liveingite from Lengenbach, Binntal, Switzerland, and the Crystal Chemistry of the Liveingite Group. *Eur. J. Miner.* **2019**, *31*, 1079–1097. [CrossRef]
83. Moelo, Y.; Orlandi, P.; Guillot-Deudon, C.; Biagioni, C.; Paar, W.; Evain, M. Lead-antimony sulfosalts from tuscany (italy). XI. The new mineral species parasterryite, $Ag_4Pb_{20}(Sb_{14.5}As_{9.5})_{\Sigma 24}S_{58}$, and associated sterryite, $Cu(Ag,Cu)_3Pb_{-19}(Sb,As)_{22}(As\text{-}As)S_{56}$, from the Pollone mine, Tuscany, Italy. *Can. Miner.* **2011**, *49*, 623–638. [CrossRef]
84. Topa, D.; Makovicky, E.; Stoeger, B.; Stanley, C. Heptasartorite, $Tl_7Pb_{22}As_{55}S_{108}$, Enneasartorite, $Tl_6Pb_{32}As_{70}S_{140}$ and Hendekasartorite, $Tl_2Pb_{48}As_{82}S_{172}$, Three Members of the Anion-Omission Series of "sartorites" from the Lengenbach Quarry at Binntal, Wallis, Switzerland. *Eur. J. Miner.* **2017**, *29*, 701–712. [CrossRef]
85. Nestola, F.; Guastoni, A.; Bindi, L.; Secco, L. Dalnegroite, $Tl_{5-x}Pb_{2x}(As,Sb)_{21-x}S_{34}$, a New Thallium Sulphosalt from Lengenbach Quarry, Binntal, Switzerland. *Miner. Mag.* **2009**, *73*, 1027–1032. [CrossRef]
86. Bindi, L.; Nestola, F.; Guastoni, A.; Secco, L. The Crystal Structure of Dalnegroite, $Tl_{5-x}Pb_{2x}(As,Sb)_{21-x}S_{34}$: A Masterpiece of Structural Complexity. *Miner. Mag.* **2010**, *74*, 999–1012. [CrossRef]
87. Topa, D.; Makovicky, E.; Dittrich, H. The Crystal Structure of 7H:12Q Cannizzarite from Vulcano, Italy. *Can. Miner.* **2010**, *48*, 483–495. [CrossRef]
88. Borisov, S.V.; Pervukhina, N.V.; Magarill, S.A.; Kuratieva, N.V.; Bryzgalov, I.A.; Mozgova, N.N.; Chaplygin, I.V. The Crystal Structure of (Cd,In)-Rich Cannizzarite from Kudriavy Volcano, Iturup Island, Kuriles, Russia. *Can. Miner.* **2012**, *50*, 387–395. [CrossRef]
89. Berlepsch, P.; Armbruster, T.; Makovicky, E.; Topa, D. Another Step toward Understanding the True Nature of Sartorite: Determination and Refinement of a Ninefold Superstructure. *Am. Miner.* **2003**, *88*, 450–461. [CrossRef]
90. Makovicky, E.; Topa, D.; Stoeger, B. The Crystal Structures of Heptasartorite, $Tl_7Pb_{22}As_{55}S_{108}$, and Enneasartorite, $Tl_6Pb_{32}As_{70}S_{140}$, Two Members of an Anion-Omission Series of Complex Sulfosalts from Lengenbach, the Swiss Alps, and Comparison with the Structures of As-Sb Sartorite Homologues. *Eur. J. Miner.* **2018**, *30*, 149–164. [CrossRef]
91. Iitaka, Y.; Nowacki, W. A Refinement of the Pseudo Crystal Structure of Scleroclase $PbAs_2S_4$. *Acta Crystallogr.* **1961**, *14*, 1291–1292. [CrossRef]
92. Robinson, S. Owyheeite. *Am. Miner.* **1949**, *34*, 398–402.
93. Laufek, F.; Pazout, R.; Makovicky, E. Crystal Structure of Owyheeite, $Ag_{1.5}Pb_{4.43}Sb_{6.0}7S_{14}$: Refinement from Powder Synchrotron X-Ray Diffraction. *Eur. J. Miner.* **2007**, *19*, 557–566. [CrossRef]
94. Stöger, B.; Gob, C.; Topa, D. A Fresh View on the Structure and Twinning of Owyheeite, a Rod-Polytype and Twofold Superstructure. *Acta Crystallogr.* **2023**, *B79*, 271–280. [CrossRef]
95. Bindi, L.; Nespolo, M.; Krivovichev, S.V.; Chapuis, G.; Biagioni, C. Producing Highly Complicated Materials. Nature Does It Better. *Rep. Progr. Phys.* **2020**, *83*, 106501. [CrossRef]
96. Biagioni, C.; Moëlo, Y.; Favreau, G.; Bourgoin, V.; Boulliard, J.-C. Structure of Pb-Rich Chabournéite from Jas Roux, France. *Acta Crystallogr.* **2015**, *B71*, 81–88. [CrossRef]
97. Matzat, E. Cannizzarite. *Acta Crystallogr.* **1979**, *B35*, 133–136. [CrossRef]
98. Bonaccorsi, E.; Merlino, S. Micro- and Mesoporous Mineral Phases. *Rev. Miner. Geochem.* **2005**, *57*, 241–290. [CrossRef]
99. Chukanov, N.V.; Aksenov, S.M.; Rastsvetaeva, R.K. Structural Chemistry, IR Spectroscopy, Properties, and Genesis of Natural and Synthetic Microporous Cancrinite- and Sodalite-Related Materials: A Review. *Micropor. Mesopor. Mater.* **2021**, *323*, 111098. [CrossRef]
100. Krivovichev, S.V. Structural and Topological Complexity of Zeolites: An Information-Theoretic Analysis. *Micropor. Mesopor. Mater.* **2013**, *171*, 223–229. [CrossRef]
101. Cámara, F.; Bellatreccia, F.; Della Ventura, G.; Mottana, A.; Bindi, L.; Gunter, M.E.; Sebastiani, M. Fantappièite, a New Mineral of the Cancrinite-Sodalite Group with a 33-Layer Stacking Sequence: Occurrence and Crystal Structure. *Am. Miner.* **2010**, *95*, 472–480. [CrossRef]
102. Bonaccorsi, E.; Ballirano, P.; Cámara, F. The Crystal Structure of Sacrofanite, the 74Å Phase of the Cancrinite–Sodalite Supergroup. *Micropor. Mesopor. Mater.* **2012**, *147*, 318–326. [CrossRef]
103. Biagioni, C.; Mauro, D.; Pasero, M.; Bonaccorsi, E.; Lepore, G.O.; Zaccarini, F.; Skogby, H. Crystal-Chemistry of Sulfates from the Apuan Alps (Tuscany, Italy). VI. Tl-Bearing Alum-(K) and Voltaite from the Fornovolasco Mining Complex. *Am. Miner.* **2020**, *105*, 1088–1098. [CrossRef]
104. Elliott, P.; Giester, G.; Rowe, R.; Pring, A. Putnisite, $SrCa_4Cr^{3+}{}_8(CO_3)_8SO_4(OH)_{16}{\cdot}25H_2O$, a New Mineral from Western Australia: Description and Crystal Structure. *Miner. Mag.* **2014**, *78*, 131–144. [CrossRef]

105. Bonaccorsi, E. The Crystal Structure of Giuseppettite, the 16-Layer Member of the Cancrinite–Sodalite Group. *Micropor. Mesopor. Mater.* **2004**, *73*, 129–136. [CrossRef]
106. Dai, Y.; Harlow, G.E. Description and Crystal Structure of Vonbezingite, a New Ca-Cu-SO_4-H_2O Mineral from the Kalahari Manganese Field, South Africa. *Am. Miner.* **1992**, *77*, 1292–1300.
107. Burns, P.C.; Deely, K.M.; Hayden, L.A. The crystal chemistry of the zippeite group. *Can. Miner.* **2003**, *41*, 687–706. [CrossRef]
108. Menchetti, S.; Sabelli, C. The Halotrichite Group: The Crystal Structure of Apjohnite. *Miner. Mag.* **1976**, *40*, 599–608. [CrossRef]
109. Plášil, J.; Dušek, M.; Novák, M.; Čejka, J.; Císařová, I.; Škoda, R. Sejkoraite-(Y), a New Member of the Zippeite Group Containing Trivalent Cations from Jáchymov (St. Joachimsthal), Czech Republic: Description and Crystal Structure Refinement. *Am. Miner.* **2011**, *96*, 983–991. [CrossRef]
110. Kampf, A.R.; Rossman, G.R.; Ma, C.; Belmonte, D.; Biagioni, C.; Castellaro, F.; Chiappino, L. Ramazzoite, $[Mg_8Cu_{12}(PO_4)(CO_3)_4(OH)_{24}(H_2O)_{20}][(H_{0.33}SO_4)_3(H_2O)_{36}]$, the First Mineral with a Polyoxometalate Cation. *Eur. J. Miner.* **2018**, *30*, 827–834. [CrossRef]
111. Krivovichev, S.V. Polyoxometalate Clusters in Minerals: Review and Complexity Analysis. *Acta Crystallogr.* **2020**, *B76*, 618–629. [CrossRef]
112. Krivovichev, S.V. Ladders of Information: What Contributes to the Structural Complexity of Inorganic Crystals. *Z. Kristallogr.* **2018**, *233*, 155–161. [CrossRef]
113. Warr, L.N. IMA–CNMNC Approved Mineral Symbols. *Miner. Mag.* **2021**, *85*, 291–320. [CrossRef]
114. Ertl, A.; Dyar, M.D.; Hughes, J.M.; Brandstaetter, F.; Gunter, M.E.; Prem, M.; Peterson, R.C. Pertlikite, a New Tetragonal Mg-Rich Member of the Voltaite Group from Madeni Zakh, Iran. *Can. Miner.* **2008**, *46*, 661–669. [CrossRef]
115. Szakall, S.; Sajo, I.; Feher, B.; Bigi, S. Ammoniomagnesiovoltaite, a new voltaite-related mineral species from Pecs-Vasas, Hungary. *Can. Miner.* **2012**, *50*, 65–72. [CrossRef]
116. Majzlan, J.; Schlicht, H.; Wierzbicka-Wieczorek, M.; Giester, G.; Poellmann, H.; Broemme, B.; Doyle, S.; Buth, G.; Koch, C.B. A Contribution to the Crystal Chemistry of the Voltaite Group: Solid Solutions, Mossbauer and Infrared Spectra, and Anomalous Anisotropy. *Miner. Petrol.* **2013**, *107*, 221–233. [CrossRef]
117. Chukanov, N.V.; Aksenov, S.M.; Rastsvetaeva, R.K.; Moehn, G.; Rusakov, V.S.; Pekov, I.V.; Scholz, R.; Eremina, T.A.; Belakovskiy, D.I.; Lorenz, J.A. Magnesiovoltaite, $K_2Mg_5Fe^{3+}{}_5Al_3(SO_4)_{12}{\cdot}18H_2O$, a New Mineral from the Alcaparrosa Mine, Antofagasta Region, Chile. *Eur. J. Miner.* **2016**, *28*, 1005–1017. [CrossRef]
118. Zhitova, E.S.; Siidra, O.I.; Belakovsky, D.I.; Shilovskikh, V.V.; Nuzhdaev, A.A.; Ismagilova, R.M. Ammoniovoltaite, $(NH_4)_2Fe^{2+}{}_5Fe^{3+}{}_3Al(SO_4)_{12}(H_2O)_{18}$, a New Mineral from the Severo-Kambalny Geothermal Field, Kamchatka, Russia. *Miner. Mag.* **2018**, *82*, 1057–1077. [CrossRef]
119. Zhitova, E.S.; Ismagilova, R.M.; Zolotarev, A.A.; Krivovichev, S.V.; Shilovskikh, V.V.; Nuzhdaev, A.A.; Nazarova, M.A. The crystal structure of magnesian halotrichite, $(Fe,Mg)Al_2(SO_4)_4\times22H_2O$: Hydrogen bonding, geometrical parameters and structural complexity. *J. Geosci.* **2023**, 68, *in press*.
120. Hazen, R.M.; Papineau, D.; Bleeker, W.; Downs, R.T.; Ferry, J.M.; McCoy, T.J.; Sverjensky, D.A.; Yang, H. Mineral evolution. *Am. Miner.* **2008**, *93*, 1693–1720. [CrossRef]
121. Hazen, R.M. Paleomineralogy of the Hadean Eon: A preliminary species list. *Am. J. Sci.* **2013**, *313*, 807–843. [CrossRef]
122. Hofmann, B.A.; Knill, M.D. Geochemistry and Genesis of the Lengenbach Pb-Zn-As-Tl-Ba-Mineralisation, Binn Valley, Switzerland. *Miner. Dep.* **1996**, *31*, 319–339. [CrossRef]
123. De Rita, D.; Funiciello, R.; Rossi, U.; Sposato, A. Structure and Evolution of the Sacrofano-Baccano Caldera, Sabatini Volcanic Complex, Rome. *J. Volcanol. Geotherm. Res.* **1983**, *17*, 219–236. [CrossRef]
124. Hong, Q.-J.; Ushakov, S.V.; Van de Walle, A.; Navrotsky, A. Melting Temperature Prediction Using a Graph Neural Network Model: From Ancient Minerals to New Materials. *Proc. Natl. Acad. Sci. USA* **2022**, *119*, e2209630119. [CrossRef]
125. Hazen, R.M.; Morrison, S.M.; Prabhu, A.; Williams, J.R.; Wong, M.L.; Krivovichev, S.V.; Bermanec, M. On the Attributes of Mineral Paragenetic Modes. *Can. J. Miner. Petrol.* **2023**, *61*, 653–673. [CrossRef]

Disclaimer/Publisher's Note: The statements, opinions and data contained in all publications are solely those of the individual author(s) and contributor(s) and not of MDPI and/or the editor(s). MDPI and/or the editor(s) disclaim responsibility for any injury to people or property resulting from any ideas, methods, instructions or products referred to in the content.